International Journal of Heat and Fluid Flow xxx (2010) xxx–xxx

Contents lists available at ScienceDirect

International Journal of Heat and Fluid Flow

journal homepage: www.elsevier.com/locate/ijhff

Fluid forces on a very low Reynolds number airfoil and their prediction

Zhou Y. [a,*], Md. Mahbub Alam [a,b], Yang H.X. [c], Guo H. [d], Wood D.H. [e,1]

[a] Department of Mechanical Engineering, The Hong Kong Polytechnic University, Hung Hom, Kowloon, Hong Kong
[b] Department of Mechanical and Aeronautical Engineering, University of Pretoria, Pretoria 0002, South Africa
[c] Department of Building Services Engineering, The Hong Kong Polytechnic University, Hung Hom, Kowloon, Hong Kong
[d] School of Aeronautical Science and Engineering, Beijing University of Aeronautics and Astronautics, Xue Yuan Road No. 37, HaiDian District, Beijing, China
[e] School of Engineering, The University of Newcastle, Callaghan NSW 2308, Australia

ARTICLE INFO

Article history:
Received 9 April 2009
Received in revised form 26 July 2010
Accepted 28 July 2010
Available online xxxx

Keywords:
Low Reynolds number airfoil
Stall of airfoil
Aerodynamics of airfoil
Reynolds number effect

ABSTRACT

This paper presents the measurements of mean and fluctuating forces on an NACA0012 airfoil over a large range of angle (α) of attack (0–90°) and low to small chord Reynolds numbers (Re_c), 5.3×10^3–5.1×10^4, which is of both fundamental and practical importance. The forces, measured using a load cell, display good agreement with the estimate from the LDA-measured cross-flow distributions of velocities in the wake based on the momentum conservation. The dependence of the forces on both α and Re_c is determined and discussed in detail. It has been found that the stall of an airfoil, characterized by a drop in the lift force and a jump in the drag force, occurs at $Re_c \geqslant 1.05 \times 10^4$ but is absent at $Re_c = 5.3 \times 10^3$. A theoretical analysis is developed to predict and explain the observed dependence of the mean lift and drag on α.

1. Introduction

The aerodynamic characteristics of airfoils at a chord Reynolds number ($Re_c = \rho c U_\infty/\mu$, where ρ and μ are the density and viscosity of the fluid, respectively, U_∞ is the free-stream velocity and c is the chord length of an aerofoil) of less than 5×10^5 are becoming increasingly important from both fundamental and industrial point of view, due to recent developments in small wind turbines, small unmanned aerial vehicles (UAVs), micro-air vehicles (MAVs), as well as researches on bird/insect flying aerodynamics (Brendel and Mueller, 1988; Hsiao et al., 1989; Dovgal et al., 1994; Lin and Pauley, 1996). For example, at the starting stage of a 500 W wind turbine, the tip Re_c increases from 1×10^4 to 1×10^5, and the angle (α) of attack reduces gradually from 86° to 20° (Ebert and Wood, 1997; Wright and Wood, 2004). A similar variation in α occurs during insect flight, but Re_c may be even lower (e.g. Wang, 2005). For UAVs and MAVs, Re_c is commonly in the range of 1×10^5 – 6×10^5. However, such low Re_c problems have not been addressed sufficiently in the literature, let alone when combined with large angle of attack. General researches on airfoil aerodynamics have focused on conventional aircraft design with Re_c beyond 5×10^5 and α below stall. Carmichael (1981), Lissaman (1983) and Mueller and DeLaurier (2003) reviewed the available low Re_c studies, with almost all the measured Re_c higher than the wind turbine values quoted above.

The aerodynamics of hovering insect flight was explored (Ellington, 1984a–e). Usherhood and Ellington (2002a,b) investigated forces acting on hawkmoth and bumblebee wings in 'propeller-like' revolution at $Re_c = 1.1 \times 10^3$–2.6×10^4. The steadily revolving wings produced high lift and drag, which was ascribed to the formation of a leading-edge vortex. Miklosovic et al. (2004) measured in a wind tunnel the lift and drag on a flipper of a humpback whale ($Re_c = 5.05 \times 10^5$–5.2×10^5). They observed that the stall angle of a flipper with a leading edge protuberance could be enlarged by approximately 40%, relatively to a flipper with a smooth leading edge, which led to increased lift and decreased drag.

In spite of their importance, the experimental lift and drag data for low Re_c are only available for some airfoils, and seldom beyond stall angle of attack. Among others, Critzos et al. (1955), Sheldahl and Klimas (1981), Michos et al. (1983) and Devinant et al. (2002) presented the test data of NACA0012 airfoil for $\alpha = 0$–90° at $Re_c = 3.6 \times 10^5$–1.8×10^6. Using force balance to measure lift and drag at $Re_c = 1 \times 10^5$–7×10^5 and $\alpha = 0$–90°, Devinant et al. (2002) showed that lift grew from zero to a maximum for increasing α between zero and stall, and then tumbled suddenly at stall, which occurred at $\alpha = 8$–20°, depending on Re_c. They further observed that lift grew with α and, after achieving the global maximum at $\alpha \approx 45°$, dropped slowly from $\alpha = 45°$ to 90°. On the other hand, drag increased monotonically with α, reaching a maximum at $\alpha \approx 90°$. Laitone (1997) measured the mean drag and lift forces successfully

* Corresponding author. Fax: +852 2365 4703.
E-mail address: mmyzhou@polyu.edu.hk (Y. Zhou).
[1] Present address: Schulich School of Engineering, University of Calgary, Canada

0142-727X/$ - see front matter © 2010 Elsevier Inc. All rights reserved.
doi:10.1016/j.ijheatfluidflow.2010.07.008

Please cite this article in press as: Zhou, Y., et al. Fluid forces on a very low Reynolds number airfoil and their prediction. Int. J. Heat Fluid Flow (2010), doi:10.1016/j.ijheatfluidflow.2010.07.008

Nomenclature

A_D	area of the airfoil (of unit length) projected on the y–z plane, $c \times \sin\alpha$
A_L	area of the airfoil (of unit length) projected on the x–z plane, $c \times \cos\alpha$
C	chord length of airfoil
C, C_0, C_1, C_2, C_3	constants in Eqs. (2), (3a$_1$), (3a$_2$), (3b$_1$), (3b$_2$), (3c$_1$), (3c$_2$), (3d$_1$), (3d$_2$), (4a), (4b), (5), and (6).
C_D, C_L	time-averaged drag and lift coefficients, $D/(c \times 0.5\rho U_\infty^2)$, $L/(c \times 0.5\rho U_\infty^2)$
C_{Drms}, C_{Lrms}	fluctuating (root-mean-square) drag and lift coefficients
D, L	mean drag and lift forces per unit length of airfoil
E_L	power spectral density functions of the lift signal
f_n	natural frequency of the airfoil-fluid system
f_v	vortex shedding frequency
K–H	Kelvin–Helmholtz
P_b	base pressure
Re_c	chord Reynolds number, $\rho U_\infty c/\mu$
S	ratio to c of distance between the leading edge and flow separation point
St	Strouhal number, $f_v c/U_\infty$
U_∞	free-stream velocity
$\overline{U}$	streamwise mean velocity
u_{rms}, v_{rms}	streamwise (x-component) and lateral (y-component) rms velocities
x, y, z	Cartesian coordinates
α	angle of attack
α_m	α corresponding to the maximum C_L
μ	viscosity of fluid
ρ	density of fluid
Superscript*	denote normalization by c and/or U_∞

at $Re_c = 2.07 \times 10^4$, though with $\alpha < 30°$. The mean drag and lift forces at the same range of α were investigated for wings with an aspect ratio of around four at $Re_c = 10^4$ by Kesel (2000), and for 20 wings of higher aspect ratio by Sunada et al. (2002) at $Re_c = 4 \times 10^3$. Selig and his co-workers have made a highly influential contribution to low-speed aerodynamics of airfoils (e.g. Selig et al., 1989, 1995, 1996; Selig and McGranahan, 2004). Selig et al. (1989) noted a peculiar drag increase at a lift coefficient of 0.5 ($Re_c = 6 \times 10^4$), where the drag coefficient reached a maximum of 0.032. They connected the observation to the laminar separation bubble, inferred from surface oil flow visualization, and referred to this drag increase as the "bubble drag". Based on their DNS data, Hoarau et al. (2003) calculated the lift and drag coefficients of NACA0012 airfoil only at $\alpha = 20°$ and $Re_c = 0.8 \times 10^3$–1.0×10^4. Although measured at $\alpha < 30°$, the mean drag and lift force data is completely absent for higher α. Furthermore, studies pertaining to the fluctuating forces on an airfoil are very scant over the whole range of α, notwithstanding the fact that the forces cause vibrations on an airfoil and acoustic noise, even leading to structural fatigue failures. As a matter of fact, these forces have already been identified as the major cause for the relatively short life and damages that occur at the tip of wind turbine blades.

Aerodynamics of an airfoil is dependent appreciably on the airfoil model, in particular, at $\alpha < 20°$, but very slightly or negligibly at $\alpha > 20°$. A symmetric NACA 0012 airfoil is used presently as a model. This type of airfoil is used not only in low Re vehicles (Murthy, 2000) but also in large transport aircraft (Tan et al., 2005), yielding a large lift and having relatively high stability due to the symmetrical shape about the centerline. Our measurements were performed at $Re_c = 5.3 \times 10^3$–5.1×10^4 and at $\alpha = 0$–$90°$ in a water tunnel. The work aims to document the lift and drag coefficients, using a highly sensitive force sensor, and to determine the dependence on α and Re_c of the time-mean lift coefficient (C_L), drag coefficient (C_D), and root-mean-square (rms) values (C_{Lrms} and C_{Drms}) of fluctuating lift and drag coefficients for a unit depth of the airfoil. Furthermore, a theoretical analysis is performed to predict C_D and C_L of an airfoil.

2. Experimental details

2.1. Test facility and setup

Experiments were conducted in a closed-loop water tunnel, with a test section of 0.3 m (width) × 0.6 m (height) × 2.4 m (length), at The Hong Kong Polytechnic University. The flow speed in the test section ranges from 0.05 m/s to 4 m/s. NACA0012 airfoil was used as the test model with a chord length of $c = 0.1$ m and a span of 0.27 m. The tests were carried out at $Re_c = 5.3 \times 10^3$–5.1×10^4, over which the free-stream turbulence level was

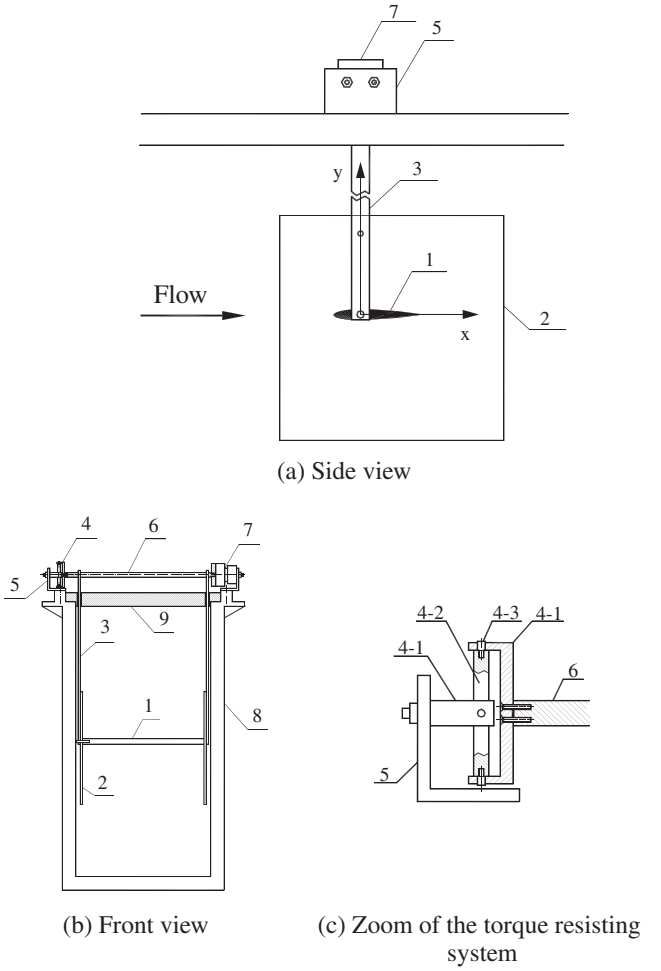

Fig. 1. Sketches of experimental setup: 1—airfoil, 2—end plates, 3—airfoil support, 4—torque-resisting system, 5—setup base, 6—connection pole, 7—load cell, 8—working section walls of water tunnel, 9—cover plate, 4–1—U-shaped connectors, 4–2—circular plate, 4–3—pins around which the connectors can turn freely.

Please cite this article in press as: Zhou, Y., et al. Fluid forces on a very low Reynolds number airfoil and their prediction. Int. J. Heat Fluid Flow (2010), doi:10.1016/j.ijheatfluidflow.2010.07.008

between 0.4% and 0.5%. This level may have an appreciable effect on the laminar boundary layer separation, which may account for, at least partly, the scattering in reported measurements at low Re_c. The α, defined to be positive in the clockwise direction (Fig. 1a), was varied from 0° to 90° with an increment step of 5° for $\alpha < 20°$ and 10° for $\alpha > 20°$.

The airfoil model spanned almost the whole width of the test section. Two square end plates, with size of 0.25 m × 0.25 m, were fixed on each end of the airfoil model with no gap between them (Fig. 1) to ensure the two-dimensionality of the flow. The leading edge of the end plate was rounded to prevent flow separation, and its trailing edge was wedge-shaped to minimize the effect of the end-plate-generated wake on flow over the airfoil.

2.2. Force measurements

In view of very low lift and drag acted on the airfoil model at the test Re_c range, a highly sensitive 3-component load cell (Kistler 9251A) including amplifiers (5011B) were used to measure the lift and drag forces. Given a pre-load to measured load ratio of larger than six, reasonably accurate force measurements may be obtained (So and Savkar, 1981). The present pre-load of the load cell was 25 kN, about 4.1×10^3 times the maximum forces measured (6 N), resulting in a very high signal-to-noise ratio in the measurement of fluid forces. As such, the present measurements are expected to yield accurate instantaneous forces. The test setup is sketched in Fig. 1. The co-ordinate system is shown in the figure, with the origin at the pivot point of the airfoil and x and y denoting the streamwise and cross-stream coordinates, respectively. The pivot was at the mid of airfoil thickness and $0.4c$ from the leading edge, which is approximately the mass center. The load cell was placed outside the test section. The force acted on the airfoil is transmitted to the sensor via two supports, marked by '3', and a connection pole, marked by '6'. The force resulted in a torque, which influenced the output of the cell. To minimize this influence, a torque-resisting system, marked by '4' (Fig. 1c), was designed, which is fixed at one end of the connection pole. The end of the connection pole on the load cell side could freely rotate relatively to the cell, thus preventing the torque from transmitting to the cell while allowing the force to be transmitted to the cell. Every joint of the system was adequately lubricated to eliminate the effects of friction.

The forces acting on the end plates and the supports (Fig. 1) were measured and subtracted to obtain the forces acting on the airfoil. The blockage effect of the airfoil at large α was corrected based on Maskell (1963). Hackett and Cooper (2001) examined in a wind tunnel a family of flat-plate wing models ($\alpha = -10°$ to 110°) with blockage ratios of 4%, 7.1%, 11.1% and 16% (presently 16.7%) and demonstrated that this correction technique worked very well for both lift and drag estimates: all corrected curves for the four blockage ratios collapse to a single line. Other factors such as static pressure gradient and the boundary layer effects were not considered, whose contribution to experimental uncertainties was negligibly small. Static calibrations of the load cell in the lift and drag directions were carried out using dead weights. The load cell is characterized by high response, resolution and stiffness, and has a high linearity in the load/output relation. The force signals were digitized using a 12-bit A/D board at a sampling frequency of 4 Hz, about 14 times the maximum (0.29 Hz) vortex shedding frequency, measured during experiments.

The natural frequency f_n of the combined airfoil-fluid system, including the load cell, needs to be measured. Furthermore, the tunnel vibration effect, if any, on the fluctuating forces must be determined in order to resolve the unsteady forces. To this end, the lift force (L) was measured using the load cell under four different conditions of the water tunnel: (i) filled with still water (the turbine was switched off), without mounting the airfoil; (ii) filled with running water (the turbine was switched on and $Re_c = 5.3 \times 10^3$), without mounting the airfoil; (iii) filled with still water, with airfoil mounted at $\alpha = 40°$ and hit slightly using a stick; (iv) filled with running water ($Re_c = 5.3 \times 10^3$), with airfoil mounted at $\alpha = 40°$. The power spectral density functions, E_L, of the lift signal are shown in Fig. 2. A comparison in E_L (Fig. 2a) between conditions (i) and (ii) suggests that there is no appreciable effect of the tunnel vibration on the load cell measurement. E_L (Fig. 2b) under condition (iii) displays a pronounced peak at 0.86 Hz, which was identified with f_n. On the other hand, under condition (iv) E_L (Fig. 2c) shows another even more pronounced peak at 0.12 Hz, which was determined to be the frequency (f_v) of vortex shedding from the airfoil, as confirmed by the power spectral density function of the LDA-measured streamwise velocity (see Section 2.3).

The peak magnitude generated at f_n, is no more than 12% of that at f_v, which is evident if E_L in Fig. 2c is re-plotted in linear scale (Fig. 2d). Note that the measured f_n may depend on the orientation of the airfoil and hence on the directions. For example, with the airfoil set at $\alpha = 0°$, 40° and 90°, f_n obtained with the test section filled with still water ($U_\infty = 0$) is 0.68, 0.86 and 1.03 Hz, respectively, in the y-direction, and 0.97, 0.86 and 0.68 Hz, respectively, in the x-direction. Interestingly, with increasing α, f_n increases in the y-direction but decreases in the x-direction. It is known that the damping force of still water on an airfoil oscillating with very small amplitude is directly proportional to the projected area of the airfoil normal to the direction of oscillation, and a higher damping force reduces f_n. Therefore, the opposite trend in the variation of f_n with α along the y- or x-direction is due to the opposite change in the projected area normal to the corresponding directions. Since the damping force is smallest at $\alpha = 90°$ along the y-direction and at $\alpha = 0°$ along the x-direction, the corresponding f_n is maximum.

2.3. LDA measurements

A two-component LDA (Dantec Model 58N40 with enhanced FVA signal processor) was deployed to measure both streamwise and lateral velocities across the airfoil wake at $x^* = 3.1$, well beyond the recirculation region even at a large α, where superscript '*' stands for normalization by c and/or U_∞. The LDA system comes with the necessary software for data processing and analysis. See Wang et al. (2006) for more details of the system. The flow was seeded using glass bubbles with a uniform diameter of 20 μm, whose density was about the same as that of water, and was specially produced for PIV or LDA measurements in water. The LDA optics was mounted on a computer-controlled three-dimensional (3-D) traversing mechanism, with a lateral traversing resolution of 1 μm. The increment between measurement points was $\Delta y^* = 0.05c$ for $\alpha \leqslant 20°$, and $0.1c$ for $\alpha \geqslant 30°$ when the wake width grew considerably.

C_D could be estimated using the conservation equation of momentum, viz.

$$C_D = 2\int_{-\infty}^{\infty} \overline{U}^*(1-\overline{U}^*)dy^* \tag{1a}$$

where $\overline{U}$ is the mean streamwise velocity. The equation is derived based on the assumption that the velocity measurement location is far enough from the airfoil so that the wake has returned to the tunnel static pressure and the rms values of streamwise and lateral velocities (u_{rms}, v_{rms}) are very small. For the velocity measurement in the near wake, where u_{rms} and v_{rms} cannot be neglected, Townsend (1956) improved the above equation by incorporating u_{rms} and v_{rms}, viz.

Please cite this article in press as: Zhou, Y., et al. Fluid forces on a very low Reynolds number airfoil and their prediction. Int. J. Heat Fluid Flow (2010), doi:10.1016/j.ijheatfluidflow.2010.07.008

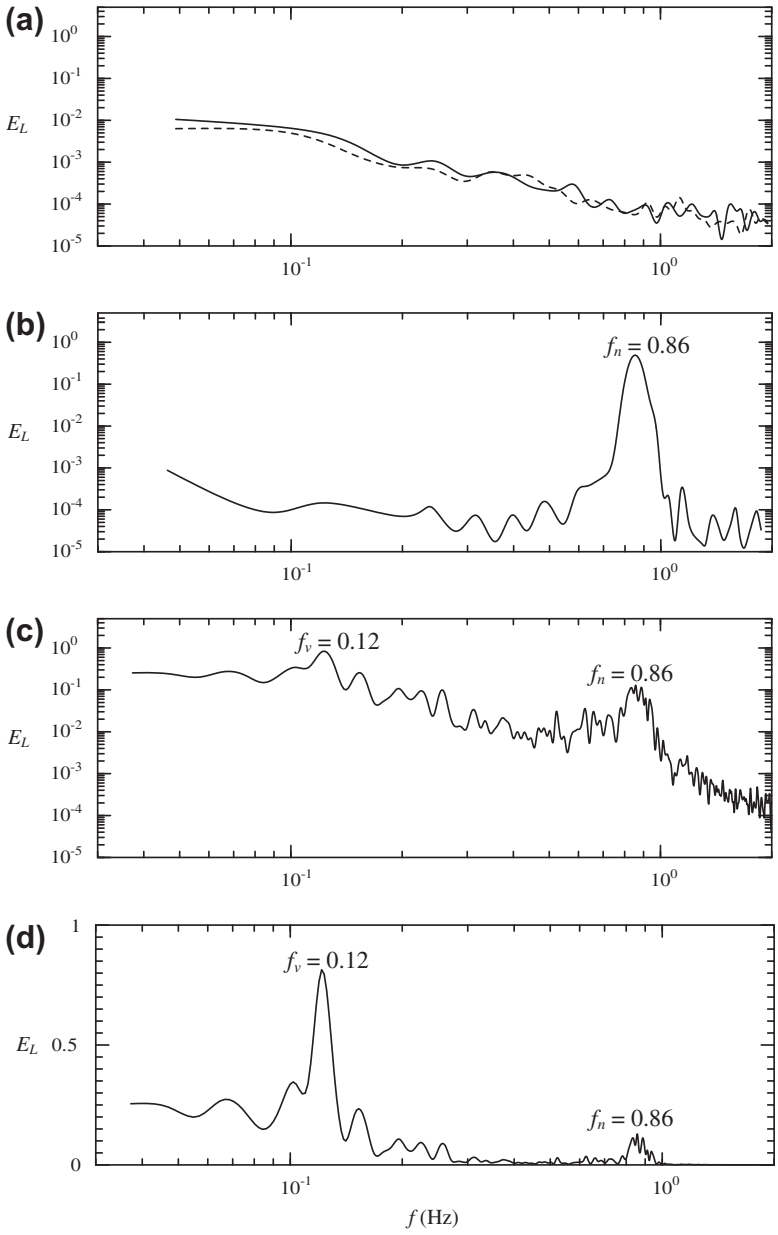

Fig. 2. Power spectral density function of the measured lift signal. (a) Tunnel full of water, without mounting the airfoil: pump switched off (no flow, broken line) and on (with flow, solid line); (b) tunnel full of water, with the airfoil mounted at $\alpha = 40°$, pump switched off (no flow); (c) pump switched on (with flow), with the airfoil mounted at $\alpha = 40°$ ($Rec = 5.3 \times 103$); (d) the same as (c), with the ordinate in the linear scale, showing the disparity in energy at f_v and f_n.

$$C_D = 2\int_{-\infty}^{\infty} \overline{U}^*(1-\overline{U}^*)dy^* + 2\int_{-\infty}^{\infty} (v_{rms}^{*2} - u_{rms}^{*2})dy^* \qquad (1b)$$

Antonia and Rajagopalan (1990) verified the validity of Eq. (1b) for a circular cylinder wake. Eq. (1b) was used to estimate C_D from the LDA-measured $\overline{U}^*$, u_{rms}^* and v_{rms}^*. Fig. 3 shows the typical lateral distributions of $\overline{U}^*$, u_{rms}^* and v_{rms}^* at $\alpha = 10°$, 30° and 50°.

2.4. LIF flow visualization

A laser-induced fluorescence (LIF) flow visualization system was used to visualize the flow at $Re_c = 5.3 \times 10^3$ and 1.05×10^3 in the (x, y) plane through mid-span of the airfoil. A 6 W argon ion laser (Spectral Physics) was used. Laser beam was transmitted by an optic fiber and transformed into a sheet using a laser-sheet probe. Dye (Rhodamine 6G 99%) in a small tank placed at about 1 m above the airfoil flew along a rubber tube into a drilled hole in the airfoil and was released into the flow at the mid-span of the airfoil through three pinholes of 1.0 mm, one at the leading edge and the other two located at $0.1c$ from the leading edge on the suction and pressure sides, respectively. A regulator valve was installed on the outlet of the tank to control the dye flow. The visualization results were recorded using a Sony video camera with a framing rate of 25 frames per second.

3. Validation of measurements

The load-cell-measured C_D on the airfoil is compared in Fig. 4 with that estimated from the momentum conservation, calculated from the LDA-measured cross-stream distributions of the mean and fluctuating velocities (Antonia and Rajagopalan, 1990). The two different estimates agree to within ±3% at $\alpha \leqslant 60°$, irrespective of Re_c. For $\alpha \geqslant 70°$, the momentum method gives a lower drag than

Please cite this article in press as: Zhou, Y., et al. Fluid forces on a very low Reynolds number airfoil and their prediction. Int. J. Heat Fluid Flow (2010), doi:10.1016/j.ijheatfluidflow.2010.07.008

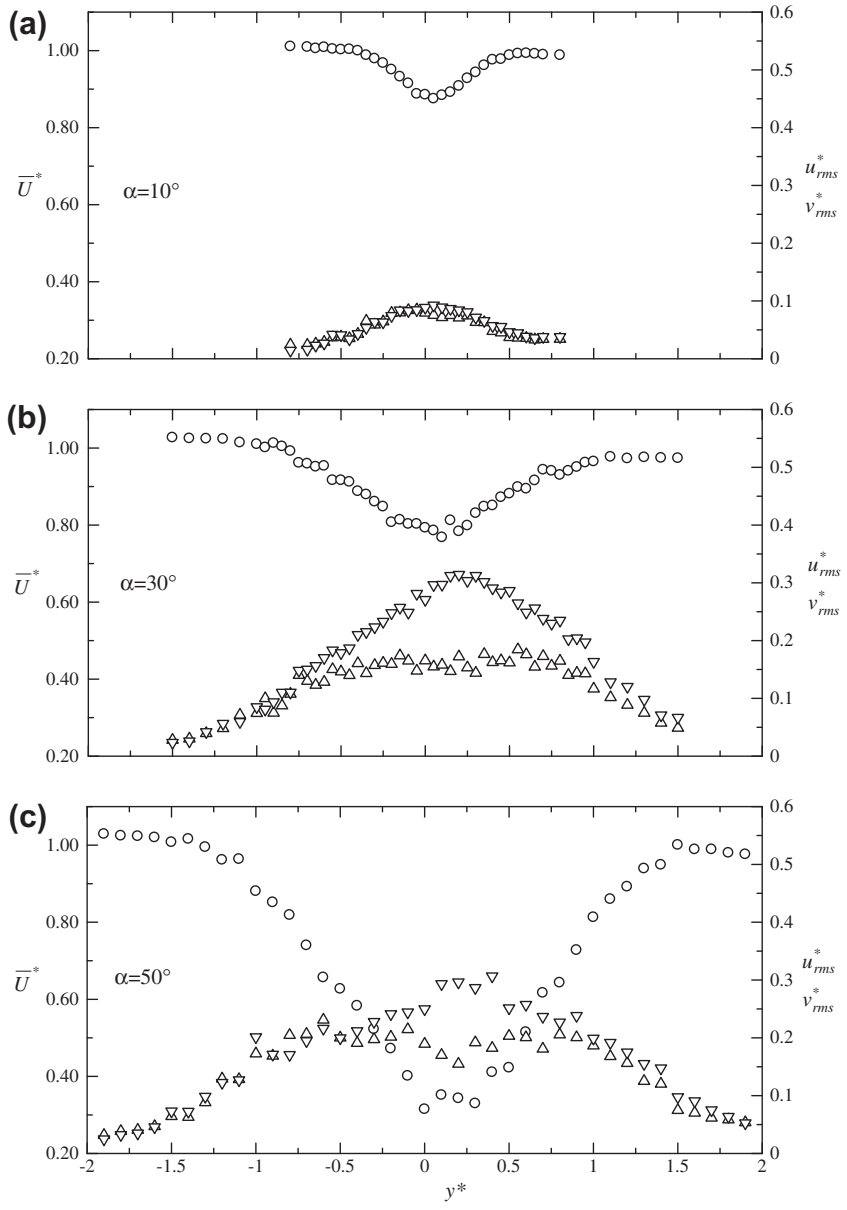

Fig. 3. LDA-measured velocities: (a) $\alpha = 10°$, (b) 30°, (c) 50°. ○, $\overline{U}^*$; u^*_{rms}; ▽, v^*_{rms}. $Re_c = 1.05 \times 10^4$.

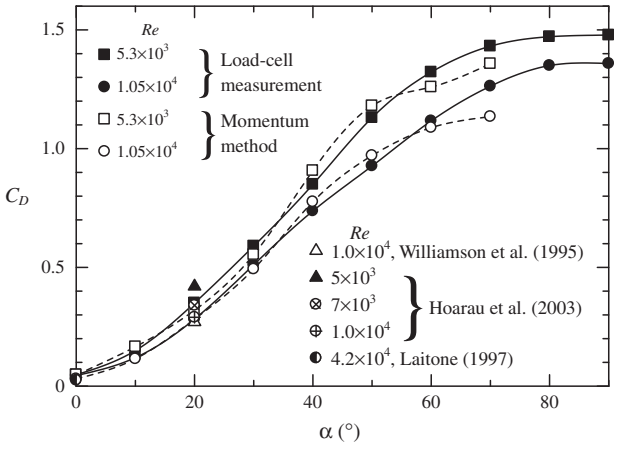

Fig. 4. Comparison between the load-cell-measured C_D and that estimated from the conservation of momentum.

the load cell measurement. At a large α, the wake is broadened so that the measured velocity profiles, limited by the test section width, could not cover the entire wake width, thus resulting in an underestimated C_D. Since the momentum conservation method is essentially two-dimensional, the good agreement between this estimate and the load cell measurement provides a strong evidence for the two-dimensionality of the flow. This agreement also provides a validation for the load cell measurement of C_D.

C_D measured by Williamson et al. (1995) was about 0.27 at $\alpha = 20°$ and $Re_c = 1.0 \times 10^4$ (see Hoarau et al., 2003), in good agreement with the present estimate ($C_D = 0.28$, $Re_c = 1.05 \times 10^4$). At the same α, Hoarau et al.'s (2003) DNS calculation (smooth flow) predicted $C_D = 0.29$, 0.34 and 0.42 at $Re_c = 1.0 \times 10^4$, 7×10^3 and 5×10^3, respectively. The first is close to our measurement at $Re_c = 1.05 \times 10^4$, the second falls in the present range of 0.28–0.35 obtained from the two different measurement methods, but the third is higher than the present estimate (0.35, $Re_c = 5.3 \times 10^3$) probably because of a difference in Re_c and the turbulent intensity. Hoarau et al.'s data at $\alpha = 20°$ indicates a decrease in C_D for higher

Please cite this article in press as: Zhou, Y., et al. Fluid forces on a very low Reynolds number airfoil and their prediction. Int. J. Heat Fluid Flow (2010), doi:10.1016/j.ijheatfluidflow.2010.07.008

Re_c for the range of Re_c given. The present measurement shows that C_D at $Re_c = 1.05 \times 10^4$ is always smaller than at $Re_c = 5.3 \times 10^3$ for a given α, re-confirming Hoarau et al.'s DNS calculation. The agreement between present and previous measurements provides another validation for the load cell measurement of C_D. It is worth mentioning that Spedding and Hedenstrom (2009) estimated C_D on a 2-D flat plate at $Re_c = 1.2 \times 10^4$ ($\alpha < 20°$) from the PIV measurement over $x^* = 2.0$–3.2 based on the conservation of momentum. Their data displays a similar trend (not shown) to the present C_D on an airfoil.

4. Measured mean drag and lift

Figs. 5 and 6 present the blockage-corrected C_L and C_D as discussed in Section 2.2, along with some published data at $Re_c = 3.6 \times 10^5$ and 7.6×10^5 measured by Sheldahl and Klimas (1981) and Michos et al. (1983), respectively. The smooth curve is a Spline curve fit to the measured data. Note that the present data at $Re_c = 5.1 \times 10^4$ is only shown for $\alpha \leqslant 40°$ because the force at $\alpha > 40°$ is relatively large, exceeding the valid range of the load cell. Evidently, C_L is dependent on Re_c for all α, growing with higher Re_c except near stall, consistent with previous reports, e.g., by Massey (1979) and Laitone (1997) for a large change in Re_c.

The stall of an airfoil is characterized by a rapid drop in C_L for a small increase in α and a burst of separation bubble, following a fully separated flow from the two edges of the airfoil. In general, the angle of attack at which stall occurs increases with Re_c, though very slowly at $Re_c > 10^6$ (Jacobs and Sherman, 1937; Marchman, 1987; Rusak et al., 2005). Fig. 5 shows the occurrence of the stall

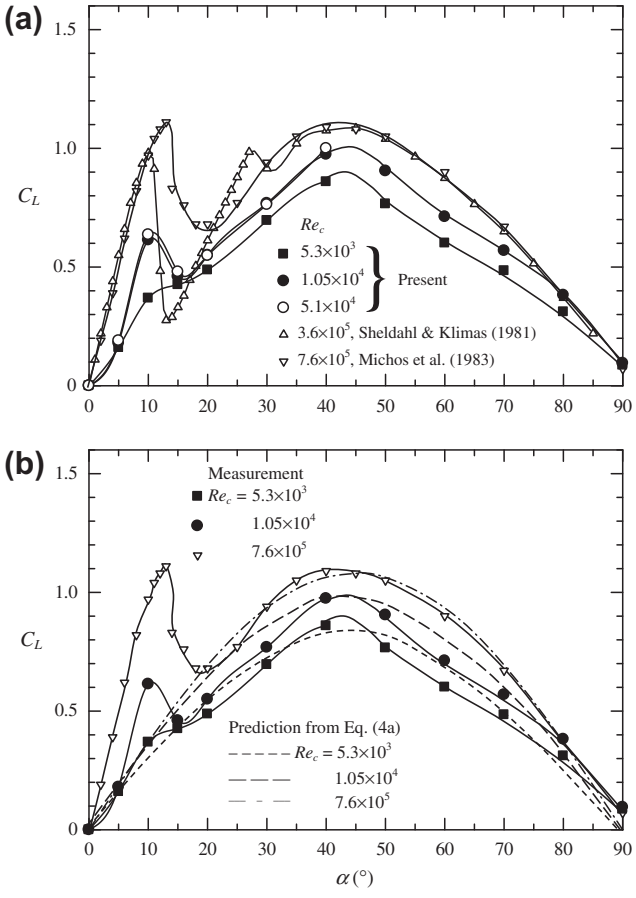

Fig. 5. Dependence of C_L on α (a) experimental measurement results, (b) comparison between experimentally obtained and theoretically predicted results.

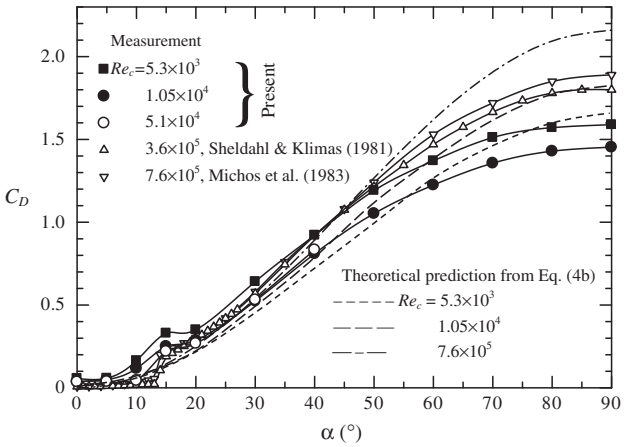

Fig. 6. Dependence of C_D on α.

at $\alpha = 12°$ and 13° for $Re_c = 3.6 \times 10^5$ and 7.6×10^5, respectively, and about 10° presently for $Re_c = 1.05 \times 10^4$ and 5.1×10^4. The stall should occur slightly either before or beyond 10°, which could not be accurately determined presently due to an increment of $\Delta\alpha = 5°$. Interestingly, the stall is absent at $Re_c = 5.3 \times 10^3$, C_L rising monotonically until $\alpha \approx 45°$, without any appreciable drop as at higher Re_c. The mechanism of stall has been previously reported at a Re_c sufficiently high to lead to the stall (e.g., Devinant et al., 2002; Mueller and DeLaurier, 2003; Larsen et al., 2007; Yang et al., 2008; Raghunathan et al., 1988). As α increases from zero to stall, a number of phenomena can be seen: (i) the separation point on the suction side moves towards the leading edge; (ii) the separated boundary layer is laminar (e.g. Laitone, 1997), though transition to turbulence in the shear layer occurs initially at the tail of the separated boundary layer and shifts towards the separation point; (iii) both C_L and C_D grow. With the stall α approached, transition to turbulence takes place near the separation point, and the separated boundary layer reattaches, forming a separation bubble. This bubble may suddenly burst, resulting in the occurrence of the stall. On the other hand, at a sufficiently low Re_c, the transition to turbulence does not occur near the separation; the separated boundary layer remains laminar for a rather long downstream distance and does not reattach. The stall will not occur without the separation bubble generated. The separated shear layer at $Re_c = 5.3 \times 10^3$ remains laminar for a longer distance and hence never reattaches on the surface for both α (Fig. 7a and c). On the other hand, the separated shear layer at $Re_c = 1.05 \times 10^4$ becomes turbulent near separation, reattaching on the surface at $\alpha = 10°$ but remaining separated at $\alpha = 15°$ (Fig. 7b and d). The result shows unambiguously that the separation bubble, which is evident at $Re_c = 1.05 \times 10^4$, is absent at $Re_c = 5.3 \times 103$, corroborating our assertion that the stall cannot occur without the formation of a separation bubble.

Beyond the stall α, C_L displays a maximum at $\alpha = \alpha_m \approx 45°$ (Fig. 5), regardless of Re_c, and then drops to about 0.08 at $\alpha = 90°$. A similar observation was made previously, e.g., by Devinant et al. (2002) and Raghunathan et al. (1988), though without explanation. One begs the question that why C_L reaches a maximum at $\alpha \approx 45°$, which will be answered in Section 5. In the post-stall region, fully separated flow prevails (e.g., Yang et al., 2008).

C_D increases monotonously with α (Fig. 6) and reaches the maximum at $\alpha = 90°$. A sudden jump in C_D at the stall α is evident at $Re_c = 3.6 \times 10^5$ or 7.6×10^5 but less so at $Re_c = 1.05 \times 10^4$ and 5.1×10^4 because of a relatively large increment in α in measurements. Below the stall α, say $\alpha < 10°$, C_D largely results from flow separation on the upper (suction) surface of the airfoil, as noted

Please cite this article in press as: Zhou, Y., et al. Fluid forces on a very low Reynolds number airfoil and their prediction. Int. J. Heat Fluid Flow (2010), doi:10.1016/j.ijheatfluidflow.2010.07.008

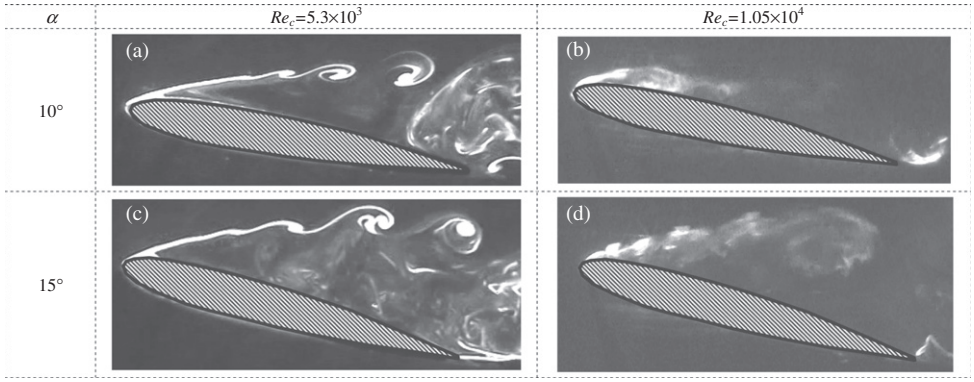

Fig. 7. Typical photographs from the LIF flow visualization, which display the presence of the separation bubble at $Re_c = 1.05 \times 10^4$ but not at $Re_c = 5.3 \times 10^3$.

in flow visualization (not shown here) and the skin friction at lower Re_c, and drops with increasing Re_c. However, at a post-stall α, the effect of Re_c on C_D is not monotonic. C_D decreases with increasing Re_c for $Re_c \geqslant 1.05 \times 10^4$, but increases for $Re_c = 5.3 \times 10^3$–1.05×10^4, which was also reported in Hoarau et al.'s (2003) DNS study ($\alpha = 20°$).

The slope of C_D, $\frac{dC_D}{d\alpha}$, may be approximated by $\frac{\Delta C_d}{\Delta_\alpha}$. Based on the measured data in Fig. 6, $\frac{\Delta C_d}{\Delta_\alpha}$ increases from $\alpha = 0°$ to 45°, and then declines till $\alpha = 90°$, that is, $\alpha = 45°$ is an inflection point of C_D (α).

5. Prediction of mean drag and lift

A linear mathematical analysis is carried out in this section to predict C_L and C_D, along with the prominent features of their dependence on α: (i) C_L reaches a maximum at $\alpha \approx 45°$ and then drops to a very small value ($\approx$0.08) at $\alpha = 90°$, (ii) C_D is maximum at $\alpha \approx 90°$, (iii) the inflection point of C_D (α) occurs at $\alpha \approx 45°$.

Note that, as α increases from 0 to 90°, the area A_L of the airfoil projected on the x-z plane shrinks following $A_L = c\cos\alpha$ given a unit spanwise length and a negligible thickness (only 12% of the chord for the NACA 0012 airfoil). The thickness may affect A_L appreciably only at $\alpha \approx 90°$. A_L is directly linked with the magnitude of the lift force. Similarly, the area A_D projected on the y–z plane could be expressed as $A_D = c\sin\alpha$, which may be connected with the magnitude of the drag force. With α increasing from 0° to 90°, the bluffness of the airfoil changes from a streamline to maximum, where bluffness is defined as the body height, i.e., $c\sin\alpha$, projected in the y–z plane. It is plausible to assume that the base pressure (P_b), defined as the pressure at the midpoint of the suction surface, increases with α and its increase, i.e., dP_b, is directly proportional to the increase in the ratio of bluffness to c, i.e., $d\{(c\sin\alpha)/c\}$, viz. $dP_b \propto d\{(c\sin\alpha)/c\}$

$$\text{or } P_b = C_1 \sin\alpha + C_2 \tag{2}$$

where C_1 and C_2 are two constants. P_b is directly linked with C_L or C_D and could be assumed to be the representative pressure for the entire base (suction) surface. As such, the mean lift L and drag D on a spanwise unit length of the airfoil could be written as $L \propto A_L P_b$ and $D \propto A_D P_b$, *viz.*

$$L = C_3 A_L P_b \tag{3a$_1$}$$

$$D = C_3 A_D P_b \tag{3a$_2$}$$

where $C_3 \neq 0$ is a proportionality constant, relating P_b and the forces. Plugging the expressions for A_D, A_L and P_b in Eqs. (3a$_1$) and (3a$_2$) yields

$$L = cC_1C_3\cos\alpha\sin\alpha + cC_2C_3\cos\alpha$$

$$D = cC_1C_3\sin\alpha\sin\alpha + cC_2C_3\sin\alpha$$

Transform L and D to C_L and C_D, respectively,

$$C_L = C_1C_3\frac{2c\sin\alpha\cos\alpha}{\rho U_\infty^2 c} + C_2C_3\frac{2c\cos\alpha}{\rho U_\infty^2 c} \tag{3b$_1$}$$

$$C_D = C_1C_3\frac{c2\sin\alpha\sin\alpha}{\rho U_\infty^2 c} + C_2C_3\frac{2c\sin\alpha}{\rho U_\infty^2 c} \tag{3b$_2$}$$

Eq. (3b) presents a general relationship of C_L or C_D with α and U_∞. For a given U_∞ or Re_c, Eq. (3b) could be rewritten as

$$C_L = C\sin 2\alpha + C_0\cos\alpha \tag{3c$_1$}$$

$$C_D = 2C\sin^2\alpha + C_0 2\sin\alpha \tag{3c$_2$}$$

$$\text{where } C = \frac{C_1C_3}{\rho U_\infty^2} \tag{3d$_1$}$$

$$\text{and } C_0 = \frac{C_2C_3}{\rho_\infty^2} \text{ are constants.} \tag{3d$_2$}$$

For a non-cambered (symmetric) airfoil such as NACA 0012, $C_L = 0$ at $\alpha = 0$. Then $C_0 = 0$ from Eq. (3c$_1$), and $C_2 = 0$ from Eq. (3d$_2$). Eq. (3c) could be reduced to

$$C_L = C\sin 2\alpha \tag{4a}$$

$$C_D = 2C\sin^2\alpha \tag{4b}$$

The constant C may be estimated from C_L or C_D measured at a post-stall α such as $\alpha = 45°$. C is presently 0.83 at $Re_c = 5.3 \times 10^3$ and 0.98 and at $Re_c = 1.05 \times 10^4$. Eq. (4a) articulates that C_L is a *sine* function of α. It is likely that C_L in Fig. 5 follows a *sine* curve except near the stall region, where the separation bubble bursts. The burst of a bubble always occurs in a discontinuous manner, resulting in a drastic change in the force coefficients (Alam et al., 2005), which is not considered in this analysis. Thus, C_L calculated from Eq. (4a) conforms well to the data at a small Re_c, i.e., 5.3×10^3, when the stall is absent.

In order to derive the α, at which a maximum or minimum C_L occurs, we differentiate Eq. (4a) with respect to α:

$$\frac{dC_L}{d\alpha} = 2C\cos 2\alpha \tag{5}$$

Let $\frac{dC_L}{d\alpha} = 0$, viz.

$$2C\cos 2\alpha = 0 \tag{6}$$

The solution to Eq. (6) is $\alpha = \alpha_m = \pm 45°$. The positive and negative values of α_m correspond to the maximum and minimum C_L, respectively, which may be confirmed from the second derivative

Please cite this article in press as: Zhou, Y., et al. Fluid forces on a very low Reynolds number airfoil and their prediction. Int. J. Heat Fluid Flow (2010), doi:10.1016/j.ijheatfluidflow.2010.07.008

of Eq. (4a). The occurrence of the maximum C_L at $\alpha = 45°$ is exactly what is observed in Fig. 5. The minimum C_L will occur if the airfoil is oriented at $\alpha = -45°$. Eq. (4a) predicts $C_L = 0$ at $\alpha = 90°$. The corresponding measurement in Fig. 5 is 0.085 at $Re_c = 5.3 \times 10^3$ and 1.05×10^4 and 0.07 at $Re_c = 3.6 \times 10^5$ and 7.6×10^5, in good agreement with the analytical results. The small departure of the measurement from the calculation (Fig. 5) could be attributed to the fact that the thickness of the airfoil has been neglected in analysis.

The predicted C_D from Eq. (4b) is in general in good agreement with the measurements (Fig. 6). There is a small departure. Eq. (4b) predicts a zero C_D at $\alpha = 0°$, whilst the corresponding measurement (Fig. 6) is 0.056, 0.038 and 0.035 for $Re_c = 5.3 \times 10^3$, 1.05×10^4 and 5.1×10^4, respectively, and 0.008 at $Re_c = 3.6 \times 10^5$ and 7.6×10^5 measured by Sheldahl and Klimas (1981) and Michos et al. (1983). This departure is ascribed to the neglected skin friction, which contributes most to C_D at $\alpha = 0°$, during the analysis. Note that for the same airfoil (NACA 0012), Laitone (1997) obtained $C_D = 0.025$ at $Re_c = 4.2 \times 10^4$ using force balance (Fig. 4).

The inflection point on C_D (α) may be predicted from Eq. (4b). Setting $\frac{d^2C_D}{d\alpha^2} = 0$ yields $\alpha = 45°$, coinciding with that from experimental data. In fact, with C evaluated from the measured C_L at $\alpha = 45°$, Eq. (4) predicts well C_D and C_L at different Re_c, except near the stall α for C_L or beyond $\alpha = 60°$ for C_D. The deviation in C_L near the stall is due to the formation of a separation bubble (e.g., Marchman, 1987), which was not considered in theoretical analysis. On the other hand, the over-estimated C_D beyond $\alpha = 60°$ is not unexpected; while the airfoil is characterized by a rounded leading edge in measurements, the one in theoretical analysis is sharp, with thickness neglected.

A number of non-linear models (Leishman, 1988; Hansen et al., 2004; Oye, 1991; Thwaites, 1960) have been previously developed to estimate C_L for small α. These models showed a lift reduction due to flow separation from the airfoil. Use C_{L0} to denote the lift on an airfoil with fully attached flow. C_{L0} is a linear function of α, valid only for very small α (e.g. $\alpha < 3°$, Laitone, 1997). With flow separated, C_L may be determined from Kirchhoff flow theory (Thwaites, 1960):

$$C_L \approx \left(\frac{1+\sqrt{S}}{2}\right) C_{L0} \tag{7}$$

where S is the ratio to c of distance between the leading edge and flow separation point, which provides a measure of flow attachment. For a fully attached flow, $S = 1$ and $C_L = C_{L0}$. With increasing α, S diminishes, and the first and second terms on the right hand side of Eq. (6) decrease and increase, respectively. Therefore, C_L increases with α, but at a smaller rate than C_{L0}. When the separation point occurs at the leading edge, $S = 0$ and $C_L \approx \frac{1}{4} C_{L0}$, that is, in a fully separated flow C_L grows with α at the same rate as in a fully attached flow. This conclusion cannot be true, for C_L climbs up to $\alpha \approx 45°$ and then retreats (Fig. 5) with its changing rate dependent on α. It is thus concluded that Eq. (6) may predict C_L only up to the stall, where the boundary layer is attached or reattached after separation from the leading edge, not beyond the stall where flow is fully separated. Beddoes (1978), Tran and Petot (1981), Leishman and Beddoes (1986a,b), Oye (1991) and Hansen et al. (2004) modeled S for the prediction of C_L only up to the stall. The presently developed equations are applicable for α beyond the stall, where the boundary layer is separated from the leading edge and the airfoil acts as a bluff body.

A remark is due on why C_L and C_D become maximum at $\alpha \approx 45°$ and 90°, respectively. As α increases from 0° to 90°, P_b grows from zero to the maximum and A_L shrinks from the maximum to zero. From (Eq. ($3a_1$)) C_L reaches its maximum at an intermediate value of α between 0° and 90°. On the other hand, both P_b and A_D grow with α and, from Eq. ($3a_2$), C_D attains its maximum at $\alpha = 90°$.

C_D is between 1.45 and 1.89 (Fig. 6), depending on Re_c, at $\alpha = 90°$ where the airfoil is like a flat plate normal to incident flow. C_D on a sharp-edged flat plate normal to incident flow is about 2 (Nakaguchi et al., 1968, $Re_c = 2 \times 10^4$–6×10^4; Bearman and Trueman, 1972, $Re_c = 2 \times 10^4$–7×10^4; Courchesne and Laneville, 1982, $Re_c = 6 \times 10^4$; Knisely, 1990, $Re_c = 720$–8.1×10^4) and almost insensitive to Re_c. On the other hand, C_D on a circular cylinder of radius R nestles between 1.1 and 1.3, depending on Re_c (e.g. Igarashi, 1984, $Re_c = 6 \times 10^4$, $C_D = 1.28$; Schewe, 1983, 4.4×10^4, 1.22; Lessage and Gartshore, 1987, 6.5×10^4, 1.19; Hover et al., 2001, 1.5×10^4–4.4×10^4, 1.2; Khalak and Williamson, 1996, 9.5×10^3, 1.15; Nebres and Batill, 1993, 3×10^3, 1.12; Alam et al., 2003a, 6.5×10^4, 1.2; Alam et al., 2003b, 5.5×10^4, 1.12). The cylinder may be considered as a plate, with both edges rounded at R and with a chord length and thickness of $2R$. Naturally, C_D for NACA 0012 airfoil, which has a rounded and a sharp edge, lies between those of circular cylinder and sharp-edged flat plate and is also sensitive to Re_c.

6. Fluctuating forces

The measured C_{Lrms} and C_{Drms} (Figs. 8 and 9) in general grow with increasing α. This is reasonable since a larger α corresponds to the increasing bluffness of the airfoil and hence the increasing size and strength of vortices separated from the airfoil. Both C_{Lrms} and C_{Drms} exhibit a local maximum at $\alpha \approx 40°$, irrespective of Re_c. In view of the course measurement increment $\Delta\alpha = 10°$, the local maximum is more likely to occur at $\alpha \approx 45°$ given a smaller $\Delta\alpha$. C_{Lrms} and C_{Drms} are higher at $Re_c = 5.3 \times 10^3$ than at $Re_c = 1.05 \times 10^4$ for all α (=0–90°) except for $\alpha = 40°$, where the difference is negligibly small. Note that C_{Lrms} is considerably higher than C_{Drms} for the same Re_c and α.

7. Reynolds number effect on forces

The Reynolds number is one of the control parameters for flow around the airfoil, and to a certain extent C_D, C_L, C_{Lrms} and C_{Drms}. How Re_c affects forces on airfoil depends on α. Figs. 10 and 11 present the dependence of C_L and C_D on Re_c at some representative α, i.e., 10°, 20°, 40° and 90°. The first α is near the stall, the second and third are beyond the stall and near the maximum C_L, respectively, and the fourth corresponds to the maximum C_D. As Re_c increases from 5.3×10^3 to 1.05×10^4, C_L displays an appreciable increase, except at $\alpha = 90°$ where the increase is rather mild (Fig. 10); meanwhile, C_D decreases (Fig. 11). Based on their DNS data, Hoarau et al. (2003) reported a decreasing C_D for increasing

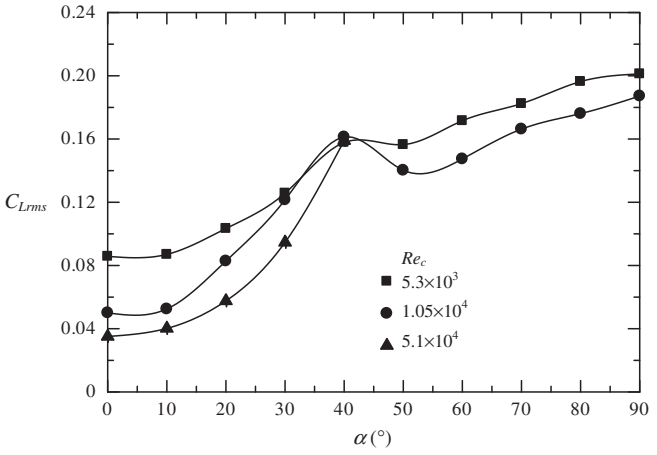

Fig. 8. Dependence of C_{Lrms} on α.

Please cite this article in press as: Zhou, Y., et al. Fluid forces on a very low Reynolds number airfoil and their prediction. Int. J. Heat Fluid Flow (2010), doi:10.1016/j.ijheatfluidflow.2010.07.008

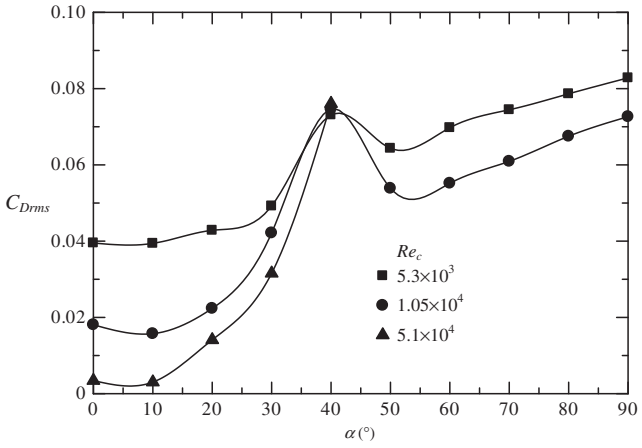

Fig. 9. Dependence of C_{Drms} on α.

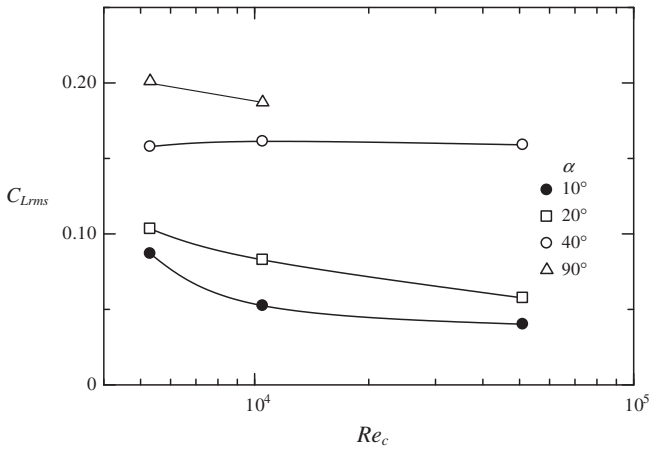

Fig. 12. Dependence of C_{Lrms} on Re_c at $\alpha = 10°$, 20°, 40° and 90°.

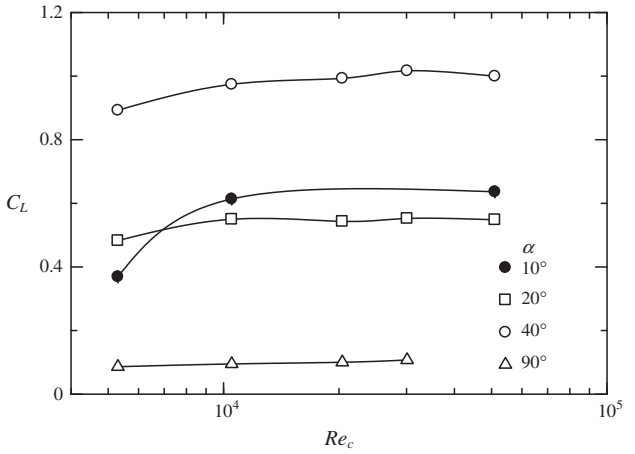

Fig. 10. Dependence of C_L on Re_c at $\alpha = 10°$, 20°, 40° and 90°.

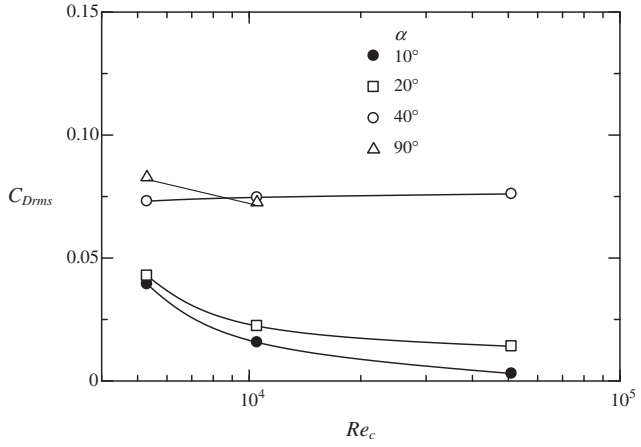

Fig. 13. Dependence of C_{Drms} on Re_c at $\alpha = 10°$, 20°, 40° and 90°.

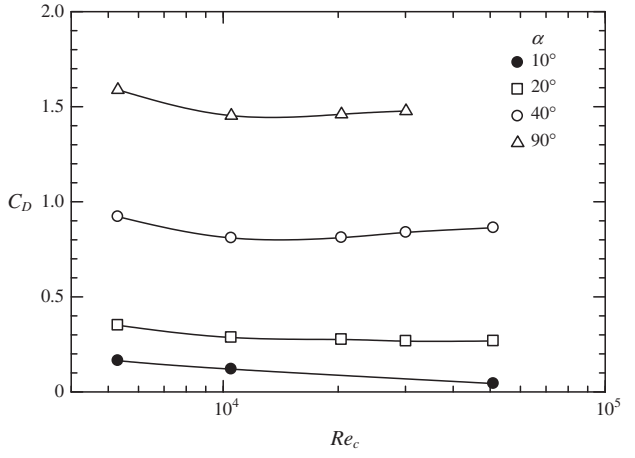

Fig. 11. Dependence of C_D on Re_c at $\alpha = 10°$, 20°, 40° and 90°.

Re_c up to 1.0×10^4 in flow over a NACA0012 airfoil at $\alpha = 20°$. A similar variation in C_D with Re_c has been well documented in a 2-D circular cylinder wake at Re (based on cylinder diameter) = 2.6×10^2–1.0×10^4, where the transition to turbulence in the shear layer moves towards the separation point with increasing Re (Zdravkovich, 1997) and even in a two-tandem circular cylinder wake at $Re = 8 \times 10^2$–2×10^3 (Xu and Zhou, 2004). Roshko (1993) and also Williamson (1996) ascribed the observation in a 2-D circular cylinder wake to the development of the 3-D flow structure during transition from laminar to turbulence. The same mechanism is responsible for the present observation in an airfoil wake.

C_L and C_D vary little for $Re_c = 1.05 \times 10^4$–5.1×10^4, particularly for $\alpha > 10°$, where the separation point occurs near the leading edge. In a circular cylinder wake of $Re = 1.05 \times 10^4$–2×10^5, where the boundary layer around the surface is laminar but the separated shear layer is turbulent, the flow separation point is almost independent of Re (Son and Hanratty, 1969; Zdravkovich, 1997). Naturally, the corresponding C_D varies little with Re (Zdravkovich, 1997; Norberg, 2003). The same could explain the weak dependence of C_D and C_L on Re_c in an airfoil wake of $Re_c = 1.05 \times 10^4$–5.1×10^4.

Both C_{Lrms} and C_{Drms} drop with increasing Re_c (Figs. 12 and 13), especially at $\alpha \leqslant 40°$ in the range of $Re_c = 5.3 \times 10^3$–1.05×10^4. The observation is ascribed to two factors: with increasing Re_c, (1) transition to turbulence in the shear layer shifts towards the separation point and (2) the separation point on the suction side moves towards the leading edge. Whilst the latter occurs only at $\alpha < 20°$, the former is appreciable up to $Re_c = 1.0 \times 10^4$ and insignificantly less so for $Re_c = 1.0 \times 10^4$–2.0×10^5, as observed in the shear layer around a 2-D circular cylinder (Zdravkovich, 1997).

8. Conclusions

An experimental study has been conducted to measure mean and fluctuating lift and drag forces on a NACA0012 airfoil at

Please cite this article in press as: Zhou, Y., et al. Fluid forces on a very low Reynolds number airfoil and their prediction. Int. J. Heat Fluid Flow (2010), doi:10.1016/j.ijheatfluidflow.2010.07.008

$\alpha = 0$–90° and $Re_c = 5.3 \times 10^3$–5.1×10^4. The dependence of the forces on α and Re_c has been examined. The following conclusions may be drawn based on present measurements.

(1) At the small Re_c, i.e. 5.3×10^3, there is no rapid drop in C_L nor a jump in C_D, suggesting the absence of the stall that is associated with an airfoil wake of $Re_c \geqslant 1.0 \times 10^4$.
(2) C_D and C_L display a strong dependence on α, as expected. C_D increases monotonically from $\alpha = 0^\circ$ to 90°, whilst C_L grows from 0 to its maximum at $\alpha \approx 45^\circ$ and then declines. The increase in C_D is rather rapid up to $\alpha = 45^\circ$ and less so beyond $\alpha = 45^\circ$. Both C_{Lrms} and C_{Drms} increase from $\alpha = 0^\circ$ to 90°, with a local maximum at $\alpha \approx 45^\circ$.
(3) A linear theoretical analysis is developed to predict the dependence of C_D and C_L on α. The analysis is consistent with the measured C_D and C_L and explains why C_L and C_D reach the maximum at $\alpha = 45^\circ$ and 90°, respectively. With α increasing from 0° to 90°, the airfoil changes from a streamlined body to a bluff body (like a normal plate). Accordingly, P_b grows from zero to the maximum and $A_L = c \times \cos\alpha$ retreats from the maximum to zero. As such, C_L reaches its maximum at an intermediate α value between 0° and 90°. On the other hand, both P_b and $A_D = c \times \sin\alpha$ grow with increasing α. Thus, C_D displays its maximum at $\alpha = 90^\circ$.
(4) The Re_c effect on C_D and C_L depends on α. As Re_c increases from 5.3×10^3 to 1.05×10^4, C_L displays an appreciable increase, except at $\alpha = 90^\circ$ where the increase is rather mild; meanwhile, C_D decreases since transition to turbulence in the shear layer moves towards the separation point. C_L and C_D vary little for $Re_c = 1.05 \times 10^4$–5.1×10^4 because of a negligibly small variation in the flow separation point. On the other hand, C_{Lrms} and C_{Drms} at $\alpha \leqslant 20^\circ$ retreat for increasing Re_c, which is more appreciable for $Re_c = 5.3 \times 10^3$–1.05×10^4. The observation is linked to the dependence on Re_c of (i) transition to turbulence in the shear layer and (ii) the occurrence of the separation point. The latter dependence is appreciable only at $\alpha \leqslant 20^\circ$.

Acknowledgements

The work described in this paper was supported by a grant from The Hong Kong Polytechnic University (Project No. G-YD83). Y.Z. wishes to acknowledge support given to him from Research Grants Council of Hong Kong Special Administrative Region through grant PolyU 5334/06E.

References

Alam, M.M., Moriya, M., Takai, K., Sakamoto, H., 2003a. Fluctuating fluid forces acting on two circular cylinders in a tandem arrangement at a subcritical Reynolds number. J. Wind Eng. Ind. Aerodyn. 91, 139–154.
Alam, M.M., Sakamoto, H., Moriya, M., 2003b. Reduction of fluid forces acting on a single circular cylinder and two circular cylinders by using tripping rods. J. Fluids Struct. 18, 347–366.
Alam, M.M., Sakamoto, H., Zhou, Y., 2005. Determination of flow configurations and fluid forces acting on two staggered circular cylinders of equal diameter in cross-flow. J. Fluids Struct. 21, 363–394.
Antonia, R.A., Rajagopalan, S., 1990. Determination of drag of a circular cylinder. AIAA J. 28, 1833–1834.
Bearman, P.W., Trueman, D.M., 1972. An investigation of the flow around rectangular cylinders. Aeronaut. Quart. 23, 229–237.
Beddoes, T.S., 1978. Onset of leading edge separation effect under dynamic conditions and low mach numbers. In: Proceedings of the 34th Annual Forum of the American Helicopter Society.
Brendel, M., Mueller, T.J., 1988. Boundary-layer measurements on an aerofoil at low Reynolds number. J. Aircraft 25, 317–612.
Carmichael, B.H., 1981. Low Reynolds Number Airfoil Survey, vol. 1. NASA CR 165803, also N82-14059.
Courchesne, J., Laneville, A., 1982. An experimental evaluation of drag coefficient for two-dimensional rectangular cylinders exposed to grid turbulence. ASME J. Fluids Eng. 104, 523–528.
Critzos, C.C., Heyson, H.H., Boswinkle, R.W., 1955. Aerodynamic characteristics of NACA 0012 airfoil section at angles of attack from 0° to 180°. NACA TN 336.
Devinant, Ph., Laverne, T., Hureau, J., 2002. Experimental study of wind-turbine airfoil aerodynamics in high turbulence. J. Wind Eng. Ind. Aerodyn. 90, 689–707.
Dovgal, A.V., Kozlov, V.V., Michalke, A., 1994. Laminar boundary layer separation: instability and associated phenomena. Prog. Aerospace Sci. 30, 61–94.
Ebert, P.R., Wood, D.H., 1997. Observations of the starting behavior of a small horizontal-axis wind turbine. Renew. Energy 12, 245–257.
Ellington, C.P., 1984a. The aerodynamics of hovering insect flight. I. The quasi-steady analysis. Philos. Trans. Roy. Soc. Lond. B 305, 1–15.
Ellington, C.P., 1984b. The aerodynamics of hovering insect flight. II. Morphological parameters. Philos. Trans. Roy. Soc. Lond. B 305, 17–40.
Ellington, C.P., 1984c. The aerodynamics of hovering insect flight. III. Kinematics. Philos. Trans. Roy. Soc. Lond. B 305, 41–78.
Ellington, C.P., 1984d. The aerodynamics of hovering insect flight. IV. Aerodynamic mechanism. Philos. Trans. Roy. Soc. Lond. B 305, 79–113.
Ellington, C.P., 1984e. The aerodynamics of hovering insect flight. VI. Lift and power requirements. Philos. Trans. Roy. Soc. Lond. B 305, 145–181.
Hackett, J.E., Cooper, K.R., 2001. Extensions to the maskell's theory for blockage effects on bluff bodies in a closed wind tunnel. Aeronaut. J. 105 (1041–1050), 409–418.
Hansen, M.H., Gaunaa, M., Madsen, H.A., 2004. A Beddoes–Leishman Type Dynamic Stall Model in State-space and Indicial Formulations. Riso-R-1354(En), Riso National Laboratory, Roskilde, Denmark.
Hoarau, Y., Braza, M., Ventikos, Y., Faghani, D., Tzabiras, G., 2003. Organized modes and the three-dimensional transition to turbulence in the incompressible flow around a NACA0012 wing. J. Fluid Mech. 496, 63–72.
Hover, F.S., Tvedt, H., Triantafyllou, M.S., 2001. Vortex-induced vibrations of a cylinder with tripping wires. J. Fluid Mech. 448, 175–195.
Hsiao, F.B., Liu, C.F., Tang, Z., 1989. Aerodynamic performance and flow structure studies of a low Reynolds number airfoil. AIAA J. 27, 129–137.
Igarashi, T., 1984. Characteristics of the flow around two circular cylinders arranged in tandem (2nd report). Bull. JSME 27, 2380–2387.
Jacobs, E.N., Sherman, A., 1937. Airfoil section characteristics as affected by variations of the Reynolds number. NACA TR, 586.
Kesel, A.B., 2000. Aerodynamic characteristics of dragonfly wing sections compared with technical airfoils. J. Exp. Biol. 203, 3125–3135.
Khalak, A., Williamson, C.H.K., 1996. Dynamics of a hydroelastic cylinder with very low mass and damping. J. Fluids Struct. 10, 455–472.
Knisely, C.W., 1990. Strouhal numbers of rectangular cylinders at incidence: a review and new data. J. Fluids Struct. 4, 371–393.
Laitone, E.V., 1997. Wind tunnel tests of wings at Reynolds numbers below 70000. Exp. Fluids 23, 405–409.
Larsen, J.W., Nielsen, S.R.K., Krenk, S., 2007. Dynamic stall model for wind turbine airfoils. J. Fluids Struct. 23, 959–982.
Leishman, J.G., 1988. Validation of approximate indicial aerodynamic functions for two-dimensional subsonic flow. J. Aircraft 25, 917–922.
Leishman, J.G., Beddoes, T.S., 1986a. A semi-empirical model for dynamic stall. J. Am. Helicopter Soc. 34, 3–17.
Leishman, J.G., Beddoes, T.S., 1986b. A generated model for airfoil unsteady aerodynamic behavior and dynamic stall using the indicial method. In: Proceedings of the 42nd Annual Forum of the American Helicopter Society.
Lessage, F., Gartshore, I.S., 1987. A method of reducing drag and fluctuating side force on bluff fodies. J. Wind Eng. Ind. Aerodyn. 25, 229–245.
Lin, J.C.M., Pauley, L.L., 1996. Low-Reynolds-number separation on an airfoil. AIAA J. 34, 1570–1577.
Lissaman, P.B.S., 1983. Low-Reynolds-number airfoils. Annu. Rev. Fluid Mech. 15, 223–239.
Marchman, J.F., 1987. Aerodynamic testing at low Reynolds numbers. J. Aircraft 24 (2), 107–114.
Maskell, E.G., 1963. Theory of blockage effects on bluff bodies and stalled wings in a closed wind tunnel. ARC R&M 3400.
Massey, B.S., 1979. Mechanics of Fluids, fourth ed. Van Nostrand Reinhold, New York.
Michos, A., Bergeles, G., Athanassiadis, N., 1983. Aerodynamic characteristics of NACA 0012 airfoil in relation to wind generators. Wind Eng. 7, 247–262.
Miklosovic, D.S., Murray, M.M., Howle, L.E., Fish, F.E., 2004. Leadingedge tubercles delay stall on Humpback Whale (Megaptera Novaeangliae) flippers. Phys. Fluids 16, L39–L42.
Mueller, T.J., DeLaurier, J.D., 2003. Aerodynamics of small vehicles. Annu. Rev. Fluid Mech. 35, 89–111.
Murthy, P.S., 2000. Low Reynolds Number Airfoil Aerodynamics. PhD thesis, Indian Institute of Science, India.
Nakaguchi, H., Hasimoto, K., Muto, S., 1968. An experimental study of aerodynamic drag on rectangular cylinders. J. Jpn. Soc. Aeronaut. Space Sci. 16, 1–5.
Nebres, J., Batill, S., 1993. Flow about a circular with a single large-scale surface perturbation. Exp. Fluids 15, 369–379.
Norberg, C., 2003. Fluctuating lift on a circular cylinder: review and new measurements. J. Fluids Struct. 17, 57–96.
Oye, S., 1991. Technical Report, Dynamic Stall Simulated as Time Lag of Separation. Department of Fluid Mechanics, Technical University of Denmark.
Raghunathan, S., Harrison, J.R., Hawkins, B.D., 1988. Thick airfoil at low Reynolds number and high incidence. J. Aircraft 25, 669–671.
Roshko, A., 1993. Perspectives on bluff body aerodynamics. J. Wind Eng. Ind. Aerodyn. 49, 79–100.
Rusak, Z., Wallace, J., Morris, W.J., 2005. On the Prediction of Stall Onset Airfoils at Moderately High Reynolds Number Flow. AIAA Paper 2005-0086, 43rd AIAA Aerospace Sciences Meeting and Exhibit, Reno, NV, January 10, 2005.

Please cite this article in press as: Zhou, Y., et al. Fluid forces on a very low Reynolds number airfoil and their prediction. Int. J. Heat Fluid Flow (2010), doi:10.1016/j.ijheatfluidflow.2010.07.008

Schewe, G., 1983. On the force fluctuations acting on a circular cylinder in cross-flow from subcritical up to transcritical Reynolds numbers. J. Fluid Mech. 133, 265–285.

Selig, M.S., Guglielmo, J.J., Broeren, A.P., Giguere, P., 1995. Summary of Low-speed Airfoil Data, vol. 1. SoarTech Publications, Virginia Beach, Virginia.

Selig, M.S., Lyon, C.A., Giguere, P., Ninham, C.P., Guglielmo, J.J., 1996. Summary of Low-speed Airfoil Data, vol. 2. SoarTech Publications, Virginia Beach, Virginia, 1996.

Selig, M.S., McGranahan, B.D., 2004. Wind tunnel aerodynamic tests of six airfoils for use on small wind turbines. Trans. ASME 126, 986-1.

Selig, M.S., Donovan, J.F., Fraser, D.B., 1989. Airfoils at Low Speeds. SoartTech Publications. H.A. Stokely, Virginia Beach, VA, USA.

Sheldahl, R.E., Klimas, P.C., 1981. Aerodynamic Characteristics of Seven Symmetrical Airfoil Sections Through 180-degree Angle of Attack for Use in Aerodynamic Analysis of Vertical Axis Wind Turbines. Sandia National Laboratories Report: SAND80-2114.

So, R.M.C., Savkar, S.D., 1981. Buffeting forces on rigid circular cylinders in cross flows. J. Fluid Mech. 105, 397–425.

Son, J.S., Hanratty, T.J., 1969. Velocity gradient at the wall for flow around a cylinder at Reynolds number from 5×10^3 to 10^5. J. Fluid Mech. 35, 353–368.

Spedding, G.R., Hedenstrom, A., 2009. PIV-based investigation of animal flight. Exp. Fluids 46 (5), 749–763.

Sunada, S., Yasuda, T., Yasuda, K., Kawachi, K., 2002. Comparison of wing characteristics at an ultralow Reynolds number. J. Aircraft 39 (2), 331–337.

Tan, J., Papadakis, M., Sampath, M.K., 2005. Computational Study of Large Droplet Breakup in the Vicinity of an Airfoil. Final Report (DOT/FAA/AR-05/42), Office of Aviation Research, Washington, DC 20591.

Thwaites, B., 1960. Incompressible Aerodynamics. Clarendon press, Oxford.

Townsend, A.A., 1956. The Structure of Turbulent Shear Flow. Cambridge University Press, Cambridge, MA (Chapter).

Tran, C.T., Petot, D., 1981. Semi-empirical model for the dynamic stall of airfoils in view of application to the calculation of the responses of a helicopter blade in forward flight. Vertica 5, 35–53.

Usherhood, J.R., Ellington, C.P., 2002a. The aerodynamics of revolving wings, I. Model hawkmoth wings. J. Exp. Biol. 205, 1547–1564.

Usherhood, J.R., Ellington, C.P., 2002b. The aerodynamics of revolving wings, II. Propeller force coefficients from mayfly to quil. J. Exp. Biol. 205, 1565–1576.

Wang, H.F., Zhou, Y., Chan, C.K., Lam, K.S., 2006. Effect of initial conditions on interaction between a boundary layer and a wall-mounted finite-length cylinder wake. Phys. Fluids 18, 065106.

Wang, Z.J., 2005. Dissecting insect flight. Annu. Rev. Fluid Mech. 37, 183–210.

Williamson, C.H.K., 1996. Vortex dynamics in the cylinder wake. Annu. Rev. Fluid Mech. 28, 477–539.

Williamson, C.H.K., Govardhan, R., Prasad, A., 1995. Experiments on Low Reynolds Number NACA0012 Airfoils. Tech. Rep. Cornell University.

Wright, A.K., Wood, D.H., 2004. The starting and low wind speed behavior of a small horizontal axis wind turbine. J. Wind Eng. Ind. Aerodyn. 92, 1265–1279.

Xu, G., Zhou, Y., 2004. Strouhal numbers in the wake of two inline cylinders. Exp. Fluids 37, 248–256.

Yang, Z., Igarashi, H., Martin, M., Hu, H., 2008. An experimental investigation on aerodynamic hysteresis of a low-Reynolds number airfoil. 46th AIAA Aerospace Science Meeting and Exhibit, January 7–10, 2008, Reno, Nevada (Paper No. AIAA-2008-0315).

Zdravkovich, M.M., 1997. Flow Around Circular Cylinders, Fundamentals, vol. 1. Oxford Science Publications.

Please cite this article in press as: Zhou, Y., et al. Fluid forces on a very low Reynolds number airfoil and their prediction. Int. J. Heat Fluid Flow (2010), doi:10.1016/j.ijheatfluidflow.2010.07.008